This is the accepted manuscript made available via CHORUS. The article has been published as:

Melting of magnesium oxide up to two terapascals using double-shock compression

L. E. Hansen, D. E. Fratanduono, S. Zhang, D. G. Hicks, T. Suer, Z. K. Sprowal, M. F. Huff, X. Gong, B. J. Henderson, D. N. Polsin, M. Zaghoo, S. X. Hu, G. W. Collins, and J. R. Rygg

Phys. Rev. B **104**, 014106 — Published 12 July 2021

DOI: 10.1103/PhysRevB.104.014106

Melting of magnesium oxide to 2 terapascals using double-shock compression

L. E. Hansen,[1,2] D. E. Fratanduono,[3] S. Zhang,[1] D. G. Hicks,[4] T. Suer,[1,5] Z. K. Sprowal,[1,2] M. F. Huff,[1,2] X. Gong,[1,6] B. J. Henderson,[1,2] D. N. Polsin,[1,6] M. Zaghoo,[1] S. X. Hu,[1,6] G. W. Collins,[1,2,6] and J. R. Rygg[1,2,6]

[1] *Laboratory for Laser Energetics, Rochester, New York 14623, USA*
[2] *Department of Physics, University of Rochester, Rochester, New York 14611, USA*
[3] *Lawrence Livermore National Laboratory, Livermore, California 94550-9234, USA*
[4] *Optical Sciences Centre, Swinburne University of Technology, Hawthorn, VIC 3122, Australia*
[5] *Department of Earth and Planetary Sciences, Harvard University, Cambridge, Massachusetts 02138, USA*
[6] *Department of Mechanical Engineering, University of Rochester, Rochester, New York 14611, USA*

(Dated: June 28, 2021)

Constraining the melting behavior of magnesium oxide, a major constituent of gaseous and rocky planets, is key to benchmarking their evolutionary models. Using a double-shock technique, we extended the MgO melt curve measurements to 2 TPa; this is twice the pressure achieved by previous melting experiments on any material. A temperature plateau is observed between 1218 and 1950 GPa in the second shock states, which is attributed to latent heat of melting. At 1950 GPa, the measured melting temperature is 17,600 K, 17% lower than recent theoretical predictions. The melting curve is steeper than that of $MgSiO_3$, indicating that MgO is likely solid in the interior of Saturn-sized gas giants and extra-solar super-Earth planets.

1. INTRODUCTION

Magnesium oxide (MgO, periclase) is an end-member of the (Mg, Fe)O magnesiowüstite mineral, a major constituent of the Earth's lower mantle[1,2]. It is likely present in the deep interiors of gas giants such as Jupiter and Saturn and in rocky extra-solar planets known as super-Earths[3,4]. As an abundant component in planets, the physical properties of MgO can influence planetary structure and evolution. The B2 phase (CsCl-type) of MgO is expected to be abundant in the mantles of super-Earths and in the rocky cores of gas giants due to the dissociation of $MgSiO_3$-perovskite[4]. The melting of MgO could therefore be an important driver of thermal and chemical exchange in the mantles and the core-mantle boundary regions of these planets[5,6]. Recent works have invoked MgO exsolution from the cores of Earth and other large rocky planets as a mechanism capable of powering a planetary magnetic dynamo[7,8]. Quantifying the melting behavior of MgO to the high pressures and temperatures of planetary interiors is therefore relevant to investigating a number of topical issues in planetary science.

The melt curve of MgO has been studied up to 40 GPa using laser- and resistance-heated multi- and diamond-anvil cells[9–12], and up to 550 GPa on the principal Hugoniot (locus of states attainable with a single shock wave) with decaying shock experiments[13,14]. Single shock waves can be used to study melting of a material to the pressure at which the principal Hugoniot crosses the melt curve; however, different experimental techniques are necessary to probe melting at higher pressures. For example, the melt curve of SiO_2 has been experimentally probed beyond the principal Hugoniot of common polymorphs fused silica and quartz using single shocks in the high-density polymorph stishovite[15]. MgO has no stable high-density polymorphs; the NaCl-type B1 phase of ambient MgO has been observed to be stable to hundreds of GPa in static-compression experiments[16]. A different experimental technique was required in order to study the high-pressure melting behavior of MgO. In this work, we apply the double-shock self-impedance match technique[17,18] to measure the melt curve of MgO to 2 TPa, the highest pressure to which any material's melt curve has been studied experimentally.

2. EXPERIMENTAL METHODS

These experiments were performed on the OMEGA EP Laser System at the Laboratory for Laser Energetics in Rochester, NY[19]. Targets consisted of a 20-μm-thick CH polystyrene ablator, a 50-μm-thick α-quartz pusher, and a 100- or 200-μm-thick single-crystal $< 100 >$ MgO sample. All pieces were laterally 3-mm squares. The target components were held together with 1–3 μm of low-viscosity epoxy. The quartz pusher served to produce steady shocks in the MgO sample and as a temperature/reflectivity reference[20,21]. Two successive shock waves were launched into the sample with a dual laser pulse through ablation of the CH. A laser pulse from an experiment and a schematic of the target stack are depicted in Fig. 1 (a). The first shock was produced with 400 J in a single laser beam with a 6- or 4-ns flattop pulse (0.067 TW or 0.1 TW); the second shock was produced with a net 1500 to 6400 J in one to three beams with a 2-ns flattop pulse (0.75 to 3.2 TW). Distributed phase plates were used to create a spatially uniform irradiance profile with a 95% encircled energy spot diameter of 1100 μm.

The time-resolved diagnostics included an SOP (streaked optical pyrometer)[22,23] and a dual-channel line-imaging VISAR (velocity interferometer system for any reflector)[24]. The SOP measured self-emission throughout the experiment in the range of 590 to 750 nm with a peak system response at 609 nm. The VISAR measured the velocity of reflecting interfaces or shock fronts with a 532-nm probe beam; the amplitude of the VISAR signal was used to determine reflectivity at 532 nm. Both VISAR

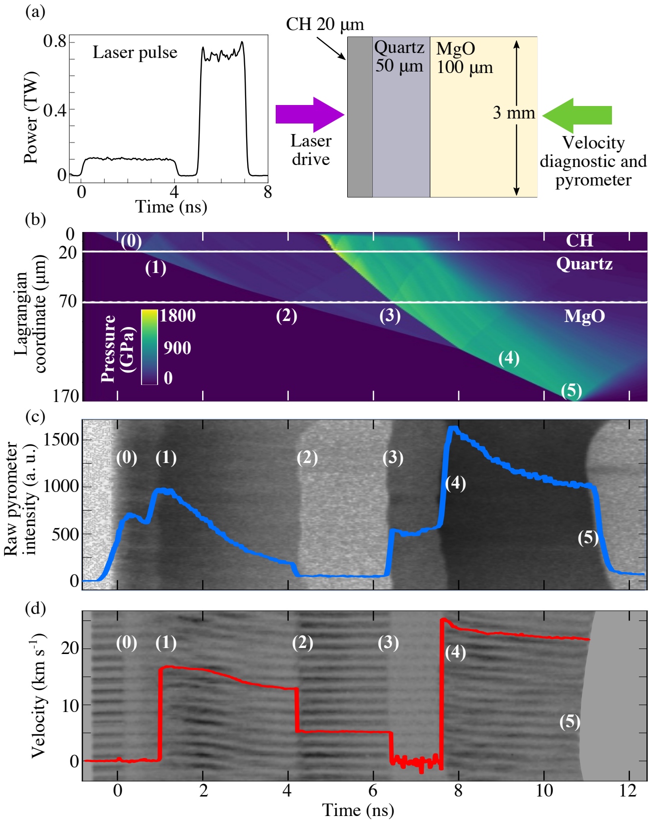

FIG. 1: (a) *Left:* The laser pulse on shot 28954. *Right:* A schematic of the target design. (b) A Lagrangian x–t diagram displaying pressure contours from a hydrodynamic simulation using the laser pulse and target in (a). (c) The raw pyrometer image from shot 28954 with the intensity over-plotted in blue. (d) The raw velocimeter image from shot 28954 with the extracted velocity over-plotted in red. The enumerated events in (b), (c), and (d) are described in the text.

and SOP have a field of view of 1-mm. Figure 1 (b) is a Lagrangian x–t diagram with pressure contours from a LILAC hydrodynamic simulation of an experiment[25]. Figure 1 (c) is an SOP image from an experiment with the raw intensity versus time over-plotted in blue; Fig. 1 (d) is the corresponding streaked VISAR image for that experiment with the extracted velocity versus time profile throughout the experiment over-plotted in red.

A sequence of events was observed in a single experiment, as enumerated in Figs. 1 (b)–(d). In region (0), the first laser pulse is launched, inducing the first shock in CH. A drop in the reflectivity is observed in VISAR, and emission from the CH ablator is measured with SOP. In region (1), the first shock enters the quartz pusher; shock velocity and emission from the shock front in quartz are measured.

In region (2), the first shock has been transmitted into the MgO sample. When the shock passes from the quartz into the higher-impedance MgO, a reshock is launched back into the quartz[26]. The emission from the reshocked quartz is absorbed by the shocked glue layer between the quartz and the MgO. The emission of the first shock in MgO is too low to observe with SOP; low signal of approximately 50 analog-to-digital units measured with SOP in region (2) is attributed to the shocked glue[27]. The quartz–MgO interface velocity is measured behind the optically transparent first shock front with VISAR; the refractive index correction and possible effects of first-shock absorption are discussed in the Supplemental Materials[27]. The first shocks in the present work range from 157 to 253 GPa. The B1 phase of MgO is experimentally shown to be stable to at least 360 GPa on the principal Hugoniot[13], which is consistent with recent theory[38]. Additionally, above 97 GPa, the elastic precursor of MgO is overdriven[39]. Therefore, the first shocks in this work exhibit no multi-wave structure.

Because the first shock in the MgO is temporally steady, the measured quartz–MgO interface velocity is equal to the particle velocity (U_{p1}) of the MgO behind the first shock front. The first shock lies on the principal Hugoniot. The pressure, density, and temperature of the B1-phase principal Hugoniot have been measured previously[39–44]. The first shock velocity was determined from U_{p1} with a previously-measured optimized linear shock velocity versus particle velocity fit[44], and the pressure, density, and internal energy of the first shock were inferred from the Rankine–Hugoniot conditions for conservation of mass, momentum, and energy across a shock front[45]. The first shock temperature was taken from the measured first shock pressure and the density functional theory pressure-temperature Hugoniot[44], which shows excellent agreement with existing MgO B1 Hugoniot temperature data[40].

In region (3), the second shock has entered the MgO sample. Transit time measurements were used to determine the average velocity of the second shock wave because the second shock was not reflective enough to be directly measured with VISAR, as seen in Fig. 1 (d), region (3). The second shock pressure, density, and internal energy are obtained by self-impedance matching at the point of shock coalescence[17,27]. The in-flight emission from the second shock in MgO is measured with SOP through the transparent first shock [Fig. 1 (c), region (3)]. A brightness temperature was inferred from this measured emission by referencing to the temperature in the quartz, which has been studied previously[20,21,27]. The brightness temperature was corrected for the reflectivity of the second shock in a grey-body model. The reflectivity of the coalesced shock served as an upper bound for the reflectivity of the second shocks[27]; this is reflected in the error bars of the temperature.

In region (4), the two shocks coalesce into a single decaying shock moving through ambient MgO. This coalesced shock wave resides on the principal Hugoniot in the liquid regime of MgO, which has been previously measured[13,14,44,46,47]. The velocity of the coalesced shock wave was measured with VISAR and corrected for the refractive index of ambient MgO at 532 nm, $n = 1.743$[48]. The corresponding particle velocity was determined from the linear shock velocity versus particle velocity fit for fluid MgO[46]. The pressure, density, and internal energy are inferred from the Rankine–Hugoniot conservation relations[45]. The reflectivity of the coalesced shock is measured with VISAR and referenced to the known quartz Hugoniot reflectivity[20,21,27]. The temperature of the coalesced shock is determined from the measured SOP emission and VISAR reflectivity, and referenced to the known quartz Hugoniot temperature[20,21,27]. At event (5), the coalesced shock wave breaks out of the MgO into vacuum.

3. RESULTS

A summary of the equation-of-state results for the present work is given in Tab. I. Coalesced shock pressures in the present work range from 1080 to 1989 GPa; corresponding second shock pressures determined from self-impedance matching are 7 to 11% higher than the coalesced shocks, ranging from 1170 to 2109 GPa. An uncertainty of 4–6% in the second shock velocity resulting from transit time measurements, propagated with a 100,000 trial Monte Carlo method, led to uncertainties in the second shock density reaching 14% but only 5% in pressure; this comes directly from the Rankine–Hugoniot conservation relations for mass and momentum. The coalesced shock reflectivity and temperature measured in this work[27] are consistent with previous results[13,14,46], lending confidence to this analysis.

The measured first (black open circles) and second (red open and closed circles) shock pressure and temperature results are plotted in Fig. 2. At a phase boundary, a material's Hugoniot is often marked by a plateau or reversal in temperature with increasing pressure as thermal energy contributes to a phase transition[49,50]. This behavior has been observed in shock experiments on diamond[51], SiO_2[21], and the principal Hugoniot of MgO[13,14]. A temperature increase in the second shock results of only 3,000 K is observed from 1.2 to 2 TPa; above this pressure, temperature rises rapidly. The three central second shock data points (closed red circles) are interpreted to lie on the melt curve of MgO because they demonstrate a lack of heating across a large increase in shock pressure, which is attributed to the latent heat of MgO melting. These experiments did not determine the structure of solid MgO, and no structural data exist at these pressures. It is assumed that the MgO melts from B2 in these experiments because no other solid phases are predicted above the B1-B2 transition.

A reflecting second shock was not measured in any of the experiments in this work, implying that solid and fluid MgO reaching 2109 GPa and 26.2 kK is a poor conductor with a reflectivity below approximately 5%. Below this threshold, the VISAR signal is expected to be dominated by ghost reflections[15] originating at the motionless MgO-vacuum interface, which have an intensity of 7% based on the refractive index of MgO. On the principal Hugoniot of MgO at 26.2 kK (968 GPa), the reflectivity has been previously measured to be 8%[13]. We would expect to be able to measure a reflectivity at the 8% level. Further experiments on the conductivity of fluid MgO on the second shock Hugoniot are necessary to resolve this open question.

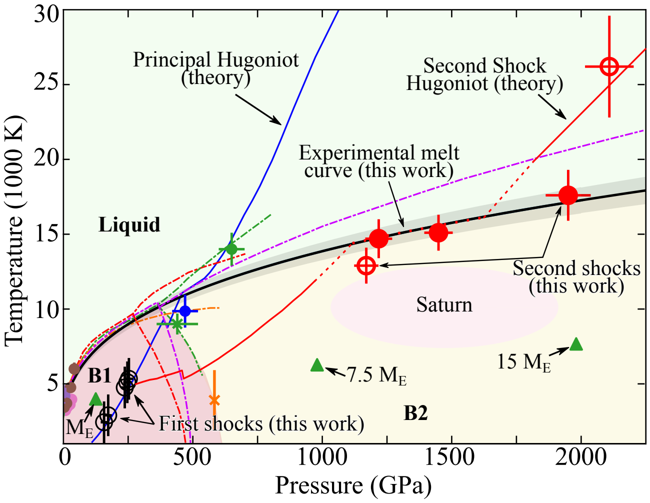

FIG. 2: The phase diagram of MgO. Black open circles represent the first shock B1 states in the present work; pressure is measured, and temperature is known from previous work[44]. Red open and closed circles are the second shock states; both pressure and temperature are measured. The three central second shock states (closed red circles) are interpreted to be on the melting curve of MgO due to a lack of heating across a large increase in pressure. Melting data from previous experiments are plotted with small closed circles circles (green[13], blue[14], pink[9], purple[11], brown[12]), and B1-B2 transition data are plotted with x's (green[13], orange[53]). Dotted-dashed curves are previously predicted phase boundaries (red[44], orange[52], purple[38], green[13]). The solid blue curve is a prediction for the principal Hugoniot[38,55,56], and the solid red curve (interpolated with dashed red) is a prediction for the second shock Hugoniot from 275 GPa[27,38,55–57]. The core–mantle boundary conditions are plotted for Saturn[58] and 1–, 7.5–, and 15–Earth-mass (M_E) super-Earths[59]. The solid black curve is Simon-Glatzel fit (Eq. 1) to the melting data in this work and lower-pressure anvil cell melt data[10,12], with grey shading representing the uncertainty in the fit parameters.

There currently exists significant discrepancy in where the principal Hugoniot of MgO crosses the B1-B2 transition and the melt curve. A large temperature reversal at 470 (40) GPa observed in decaying shock experiments[14] was attributed to MgO melting (blue circle). In earlier, and nearly identical, decaying shock experiments[13], the observed temperature reversal at 440 (80) GPa was attributed to the B1-B2 transition (green x), while a small slope change in the Hugoniot at 650 (50) GPa was attributed to melting (green circle). Density functional theory (DFT) methods (red dotted-dashed curves) predict a steep melting curve[44] consistent with the interpretation of melt at 650 GPa[13]. However, the principal Hugoniot of MgO crosses that DFT predicted B1-B2 transition at 300 GPa, while the experimentally observed temperature reversal occurs closer to 450 GPa. Older first principles molecular dynamics studies[52] (pink dotted-dashed curve)

Shot	U_{p1}(km/s)	P_1(GPa)	U_{sC}(km/s)	P_C(GPa)	U_{s2}(km/s)	P_2(GPa)	ρ_2(g/cm^3)	T_2(1000 K)
29751	5.12 (0.12)	247 (7)	23.18 (0.14)	1080 (20)	27.15 (0.8)	1170 (41)	8.65 (0.3)	12.9 (1.2)
29749	4.98 (0.12)	237 (7)	23.72 (0.14)	1142 (21)	26.58 (1.1)	1218 (39)	9.13 (0.4)	14.7 (1.3)
28954	5.21 (0.12)	253 (7)	25.39 (0.14)	1344 (23)	28.38 (0.7)	1449 (37)	9.53 (0.3)	15.1 (1.2)
30307	3.76 (0.12)	157 (6)	28.47 (0.14)	1761 (28)	31.01 (1.7)	1950 (87)	9.94 (1.0)	17.6 (1.7)
30306	4.02 (0.12)	173 (6)	30.01 (0.14)	1989 (31)	30.00 (1.5)	2109 (74)	11.84 (1.2)	26.2 (3.4)

TABLE I: Equation-of-state results for double-shocked MgO. U_{p1} is the steady first shock particle velocity. U_{s2} and U_{sC} are the second shock velocity and coalesced shock velocity at the self-impedance match[17] point (the point of shock coalescence). The first shock pressure P_1 and coalesced shock pressure P_C are determined from previous results[44,46], and the second shock pressure P_2 and density ρ_2 are obtained by self-impedance matching. The second shock temperature is measured with an optical pyrometer. All velocities are given in the lab frame.

predict a gentle melt slope consistent with the melting interpretation at 470 GPa[14]. The most recent density functional molecular dynamic calculations[38] (purple dotted-dashed curves) predict that the principal Hugoniot crosses the melt curve at 550 GPa—this is between the interpretation of melting pressure from both decaying shock experiments[13,14]. Furthermore, x-ray diffraction experiments on ramp compressed MgO measure the B1-B2 phase transition at 582 (10) GPa[53] (orange x); this is higher pressure than predicted by any model for the B1-B2 transition.

To capture the shape of the high pressure melt curve, we performed a fit to our data combined select lower-pressure anvil cell melting data[10,12] with a Simon–Glatzel equation of the form:

$$T_m[K] = 3098\Big(\frac{P_m[GPa]}{a} + 1\Big)^{1/b} \qquad (1)$$

where T_m and P_m are the temperature and pressure of the melt curve, and 3098 K is the melting temperature of MgO at atmospheric pressure[10]. This empirical relation has been used to describe the melting behavior of other oxides including SiO_2[15] and $MgSiO_3$[54]. The best fit parameters are given by $a = 9.15 \pm 2.23$ GPa and $b = 3.14 \pm 0.19$ with a covariance of -0.39, determined from a non-linear least squares analysis. A previously published melting curve of MgO[15] based on extrapolation of anvil cell and decaying shock melting data[10,11,13] overestimates the melting temperature at 1950 GPa by 27%. The fit in Eq. 1 does not allow for a change in slope at the B1-B2-liquid triple point; the pressure and temperature of the triple point have not been measured, and theoretical approaches disagree on its location. The decaying shock melting data[13,14] were not included in this fit because of the disagreement in interpretation of experiments as discussed above. This simple fit was chosen based on the discrepancy in the melting temperature of MgO on the principal Hugoniot. Fits based on different interpretations of the previous decaying shock work[13,14], and on different predicted locations of the triple point, are discussed in the Supplemental Materials[27].

The melt curve in Eq. 1 is plotted in Fig. 2 (solid black) and shows strong agreement with recent density functional theory[38] (dotted-dashed purple curve) up to 650 GPa before the curves diverge. Reference[38] overestimates the measured melting temperature at 1950 GPa by 17%. The highest-pressure second shock equation-of-state point in this work is in the liquid regime of the 173 GPa secondary Hugoniot of MgO and shows general agreement with First-Principles Equation of State simulations of secondary Hugoniots from similar initial shock conditions[55–57]; the slope of the secondary Hugoniot defined by the two highest-pressure second shock points in this work does appear steeper than theoretical predictions. The discrepancy between experiment and theory on the melt curve could originate from the complex elastic and plastic responses of MgO during the shock/reshock and phase transformation processes, which have not been taken into account in the first principles calculations. This calls for larger-scale non-equilibrium simulations and crystallographic diagnostics to better understand problems as such. The low-pressure second-shock data in this work demonstrate that the double-shock technique is a valuable method for probing the behavior of MgO in the solid phase at the temperatures and pressures directly relevant to the core–mantle boundary of gas giants similar in size and composition to Saturn[58] and super-Earths in the 7.5 to 15–Earth-mass range[59].

4. IMPLICATIONS

A key implication of our results is that pure MgO could exist as a solid at the pressure-temperature conditions inside a Saturn-sized gas giant. As shown in Fig. 3, MgO has a steeper melting curve than other abundant planetary materials including SiO_2[15], $MgSiO_3$[54,60], diamond[51], Fe[61,62], FeO[63–65], and H_2O[66,67]. However, mixing with other materials (e.g., MgO-FeO-SiO2) could depress the melting temperature and result in liquid MgO mixtures inside planets[68]. MgO has a steeper melt curve than $MgSiO_3$ above 150 GPa, indicating that the pressure-induced dissociation of liquid $MgSiO_3$ predicted to occur at 10,000 K and 1 TPa[4] would likely result in a solid MgO layer inside Saturn-sized gas giants. Since the solid B2-phase MgO is only weakly soluble in fluid hydrogen, Saturn's core could have remained stable throughout its evolution, i.e. not eroded, as is thought to be the case for larger gas giants such as Jupiter[69].

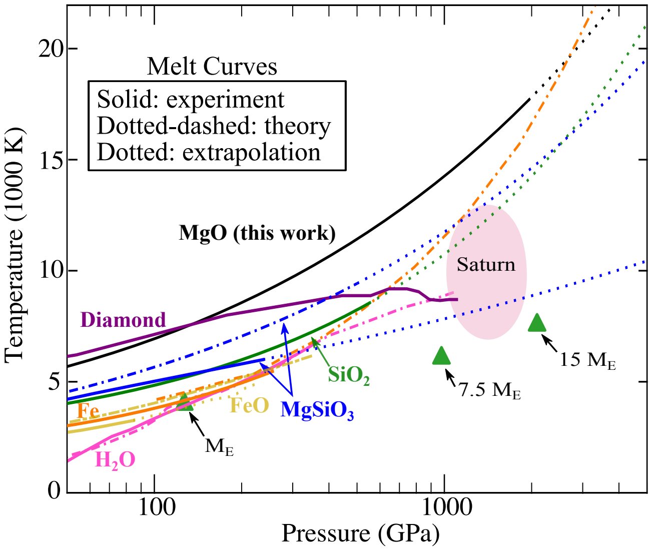

FIG. 3: A comparison of melt curves of planetary materials. Diamond: experiment (solid purple[51]). SiO_2: experiment and extrapolation (solid and dotted green[15]). $MgSiO_3$: experiment (solid blue[54]), theory (dotted-dashed blue[60]), and extrapolations (dotted blue). Fe: experiment (solid orange[61]) and theory (dotted-dashed orange[62]). FeO: experiment (solid yellow[63]), extrapolation (dotted yellow[64]), and theory (dotted-dashed yellow[65]). H_2O superionic melt: experiment (solid pink[66]) and theory (dotted-dashed pink[67]). The present experimental work on MgO (solid black, extrapolated with dotted black) represents the highest pressure to which a melt curve has ever been measured. The core–mantle boundary conditions are plotted for Saturn[58] and 1–, 7.5–, and 15–Earth-mass (M_E) super-Earths[59].

The results of the current study are also relevant to rocky planet formation and evolution processes. The extreme pressures and temperatures generated by giant impacts during terrestrial planet formation can cause significant melting and mixing of MgO with metallic Fe[70]. Dissolution of Mg into Fe could have planet-scale consequences if transported to the cores of terrestrial planets. MgO could exsolve from cores upon cooling, potentially providing enough energy to power a geodynamo and generate a planetary magnetic field[7,8]. Alternatively, if metallic, MgO could remain dissolved in Fe cores resulting in a layered core structure[71].

To fully understand the diversity of planetary structures and processes, it is imperative to further quantify the melting behavior of oxides and oxide mixtures to the extreme conditions of the current study. An MgO-rich layer could strongly influence thermal convection in both gas giants or super-Earths through enhancement of thermal conductivities[72]. MgO is known to exist as a binary solution with FeO at conditions of Earth's interior[12,73]. The results of recent laser-driven compression experiments suggest that ferropericlase (a solid solution composed of MgO and FeO) could exist as a stable B2 structure above 530 GPa[74]. However, the melting behaviors of ferropericlase and FeO have been experimentally quantified only up to 120 GPa[73] and 77 GPa[63] respectively. Future experiments on MgO and FeO mixtures will help elucidate the importance of these materials on melting, rheological, and transport properties in the interiors of super-Earths and gas giants.

5. CONCLUSION

In summary, laser-driven double-shock compression is a valuable method for probing the behavior of MgO in the solid phase at extreme conditions. The present work uses this technique to extend the melting curve of MgO up to 2 TPa and 20,000 K, the highest pressures and temperatures to which any material's melt curve has been probed experimentally. These measurements allowed us to explore the state of the deep interiors of Saturn-sized gas giants and super-Earths. The technique can be used to further quantify the melting behavior of other planetary materials to further investigate the diversity of planetary structures. Additionally, the technique presented in this work will lead to new advances in probing phase transitions of transparent materials up to TPa pressures and significantly advance warm dense matter physics.

Acknowledgments

This material is based upon work supported by the Department of Energy National Nuclear Security Administration under Award Number DE-NA0003856, the University of Rochester, the New York State Energy Research and Development Authority, the NSF Physics Frontier Center award PHY-2020249, and the Australian Research Council grant FT140101104. Lawrence Livermore National Laboratory is operated by Lawrence Livermore National Security, LLC, for the U.S. Department of Energy, National Nuclear Security Administration under Contract DE-AC52-07NA27344. The Lawrence Livermore National Laboratory AnalyzeVISAR code written by J. H. Eggert, R. S. McWilliams, D. E. Fratanduono, and M. Millot was used to process part of the VISAR and SOP data. The authors thank M. Ginnane of the University of Rochester Mechanical Engineering Department and the Laboratory for Laser Energetics for her work on the calibration of the SOP system on OMEGA EP.

This report was prepared as an account of work sponsored by an agency of the U.S. Government. Neither the U.S. Government nor any agency thereof, nor any of their employees, makes any warranty, express or implied, or assumes any legal liability or responsibility for the accuracy, completeness, or usefulness of any information, apparatus, product, or process disclosed, or represents that its use would not infringe privately owned rights. Reference herein to any specific commercial product, process, or service by trade name, trademark, manufacturer, or otherwise does not necessarily constitute or imply its endorsement, recommendation, or favoring by the U.S. Government or any agency thereof. The views and opinions of authors expressed herein do not necessarily state

or reflect those of the U.S. Government or any agency thereof.

---

[1] W. F. McDonough and S.-s. Sun, Chem. Geol. **120**, 223 (1995).

[2] J.-Fu. Lin, D. L. Heinz, H.-k. Mao, R. J. Hemley, J. M. Devine, J. Li, and G. Shen, Proc. Natl. Acad. Sci. **100**, 4405 (2003).

[3] S. Seager, M. Kuchner, C. A. Hier-Majumder, and B. Militzer, Astrophys. J. **669**, 1279 (2007).

[4] K. Umemoto, R. M. Wentzcovitch, and P. B. Allen, Science **311**, 983 (2006)

[5] L. Strixude, Phil. Trans. R. Soc. A **372**, 20130076 (2014).

[6] W. B. Tonks and H. J. Melosh, J. Geophys. Res. **98**, 5319 (1993).

[7] J. Badro, J. Siebert, and F. Nimmo, Nature **536**, 326 (2016).

[8] J. G. O'Rourke and D. J. Stevenson, Nature **529**, 387 (2016).

[9] A. Zerr and R. Boehler, Nature **371**, 506 (1994).

[10] L. S. Dubrovinsky and S. K. Saxena, Phys. Chem. Miner. **24**, 547 (1997).

[11] L. Zhang and Y. Fei, Geophys. Res. Lett. **35** (2008).

[12] Z. Du and K. K. M. Lee, Geophys. Res. Lett. **41**, 8061 (2014).

[13] R. S. McWilliams, D. K. Spaulding, J. H. Eggert, P. M. Celliers, D. G. Hicks, R. F. Smith, G. W. Collins, and R. Jeanloz, Science **338**, 1330 (2012).

[14] R. M. Bolis, G. Morard, T. Vinci, A. Ravasio, E. Bambrink, M. Guarguaglini, M. Koenig, R. Musella, F. Remus, J. Bouchet et al., Geophys. Res. Lett. **43**, 9475 (2016).

[15] M. Millot, N. Dubrovinskaia, A. ernok, S. Blaha, L. Dubrovinsky, D. G. Braun, P. M. Celliers, G. W. Collins, J. H. Eggert, and R. Jeanloz, Science **347**, 418 (2015).

[16] T. S. Duffy, R. J. Hemley, and H. K. Mao, Phys. Rev. Lett. **74**, 1371 (1995).

[17] M. Guarguaglini, J.-.A. Hernandez, A. Benuzzi-Mounaix, R. Bolis, E. Brambrink, T. Vinci, and A. Ravasio, Phys. Plasmas **26**, 042704 (2019).

[18] M. Guarguaglini, F. Soubiran, J.-A. Hernandez, A. Benuzzi-Mounaix, R. Bolis, E. Brambrink, T. Vinci, and A. Ravasio, Nat. Comm. **12**, 840 (2021).

[19] D. D. Meyerhofer, J. Bromage, C. Dorrer, J. H. Kelly, B. E. Kruschwitz, S. J. Loucks, R. L. McCrory, S. F. B. Morse, J. F. Myatt, P. M. Nilson et al., J. Phys.: Conf. Ser. **244**, 032010 (2010).

[20] S. Brygoo, M. Millot, P. Loubeyre, A. E. Lazicki, S. Hamel, T. Qi, P. M. Celliers, F. Coppari, J. H. Eggert, D. E. Fratanduono et al., J. Appl. Phys. **118**, 195901 (2015).

[21] D. G. Hicks, T. R. Boehly, J. H. Eggert, J. E. Miller, P. M. Celliers, and G. W. Collins, Phys. Rev. Lett. **97**, 025502 (2006).

[22] J. E. Miller, T. R. Boehly, A. Melchior, D. D. Meyerhofer, P. M. Celliers, J. H. Eggert, D. G. Hicks, C. M. Sorce, J. A. Oertel, and P. M. Emmel, Rev. Sci. Instrum. **78**, 034903 (2007).

[23] M. C. Gregor, R. Boni, A. Sorce, J. Kendrick, C. A. McCoy, D. N. Polsin, T. R. Boehly, P. M. Celliers, G. W. Collins, D. E. Fratanduono, J. H. Eggert, and M. Millot, Rev. Sci. Instrum. **87**, 114903 (2016).

[24] P. M. Celliers, D. K. Bradley, G. W. Collins, D. G. Hicks, T. R. Boehly, and W. J. Armstrong, Rev. Sci. Instrum. **75**, 4916 (2004).

[25] J. Delettrez, R. Epstein, M. C. Richardson, P. A. Jaanimagi and B. L. Henke, Phys. Rev. A **36**, 3926 (1987).

[26] R. G. McQueen, S. P. Marsh, J. W. Taylor, J. N. Fritz, and W. J. Carter, in *High-Velocity Impact Phenomena*, edited by R. Kinslow (Academic Press, New York, 1970).

[27] See the Supplemental Material at [link], which includes Refs.[28–37].

[28] G. D. Stevens, L. R. Veeser, P. A. Rigg, & R. S. Hixson. *AIP Conf. Proc.* **845**, 1353 (2006).

[29] J. Wackerle, H. L. Stacy, and J. C. Dallman, *Proc. SPIE* **832**, 72 (1987).

[30] D. Hayes, *J. Appl. Phys.* **89**, 6484 (2001).

[31] J. Li, X. Zhou, & J. Li. *Rev. Sci. Instrum.* **79**, 123107 (2008).

[32] D. E. Fratanduono (private communication)

[33] L. He, M. J. Tang, M. F. Zeng, X. M. Zhou, W. J. Zhu, and F. S. Liu, *Physica B* **410**, 137 (2013).

[34] M. Knudson, J. Asay, and C. Deeney, *J. Appl. Phys.* **97**, 073514 (2005).

[35] D. Cebulla and R. Redmer, Phys. Rev. B **89**, 134107 (2014).

[36] S. Zhang, R. Paul, M. A. Morales, F. Malone, and S. X. Hu, in preparation.

[37] J. C. Wheeler, J. Chem. Phys. **61**, 4474 (1974).

[38] F. Soubiran and B. Militzer, Phys. Rev. Lett. **125**, 175701 (2020).

[39] D. E. Fratanduono, J. H. Eggert, M. C. Akin, R. Chau, and N. C. Holmes, J. Appl. Phys. **114**, 043518 (2013).

[40] B. Svendsen and T. J. Ahrens, Geophys. J. Int. **91**, 667 (1987).

[41] M. S. Vassiliou and T. J. Ahrens, Geophys. Res. Lett. **8**, 729 (1981).

[42] T. S. Duffy and T. J. Ahrens. J. Geophys. Res. Solid Earth **100**, 529 (1995).

[43] L. Zhang, Z. Gong, and Y. Fei, J. of Phys. and Chem. Solids **69**, 2344 (2008).

[44] S. Root, L. Shulenburger, R. W. Lemke, D. H. Dolan, T. R. Mattsson, and M. P. Desjarlais, Phys. Rev. Lett. **115**, 198501 (2015).

[45] Ya. B. Zeldovich and Yu. P. Razer, in *Physics of Shock Waves and High-Temperature Hydrodynamic Phenomena*, edited by W. D. Hayes and R. F. Probstein (Dover Publications, Mineola, NY, 2002).

[46] C. A. McCoy, M. C. Marshall, D. N. Polsin, D. E. Fratanduono, P. M. Celliers, D. D. Meyerhofer, and T. R. Boehly, Phys. Rev. B **100**, 014106 (2019).

[47] K. Miyanishi, Y. Tange, N. Ozaki, T. Kimura, T. Sano, Y. Sakawa, T. Tsuchiya, and R. Kodama, Phys. Rev. E **92**, 023103 (2015).

[48] R. E. Stephens and I. H. Malitson, J. Res. Natl. Bur. Stand. **49**, 249 (1952).

[49] S. B. Kormer, Sov. Phys.-Usp. **11**, 229 (1968).

[50] G. Lyzenga, T. J. Ahrens, and A. C. Mitchell, J. Geophys. Res. **88**, 2431 (1983).

[51] J. H. Eggert, D. G. Hicks, P. M. Celliers, D. K. Bradley, R. S. McWilliams, R. Jeanloz, J. E. Miller, T. R. Boehly, and G. W. Collins, Nat. Phys. **6**, 40 (2010).

[52] N. de Koker and L. Stixrude, Geophys. J. Int. **178**, 162

(2009).

[53] F. Coppari, R. F. Smith, J. H. Eggert, J. Wang, J. R. Rygg, A. Lazicki, J. A. Hawreliak, G. W. Collins, and T. S. Duffy, Nat. Geosci. **6**, 926 (2013).

[54] D. E. Fratanduono, M. Millot, R. G. Kraus, D. K. Spaulding, G. W. Collins, P. M. Celliers, and J. H. Eggert, Phys. Rev. B **97**, 214105 (2018).

[55] F. Soubiran, F. Gonzalez-Cataldo, K. P. Driver, S. Zhang, and B. Militzer, J. Chem. Phys. **151**, 214104 (2019).

[56] B. Militzer, F. Gonzalez-Cataldo, S. Zhang, K. P. Driver, and F. Soubiran, Phys. Rev. E **103**, 013203 (2021).

[57] The principal and the second-shock Hugoniots at 20,000 K or higher are calculated by using the first-principles equation of state (FPEOS) database published in Refs.[55,56] for MgO. The initial conditions for the second shocks are estimated following the approach of S. Zhang, R. Paul, M. A. Morales, F. Malone, and S. X. Hu, in preparation. See the supplemental material for details.

[58] F. Gonzalez-Cataldo, H. F. Wilson, and B. Militzer, Astrophys. J. **787**, 79 (2014).

[59] F. W. Wagner, N. Tosi, F. Sohl, H. Rauer, and T. Spohn, Astron. Astrophys. **541**, A103 (2012).

[60] Y. Fei, C. T. Seagle, J. P. Townsend, C. A. McCoy, A. Boujibar, P. Driscoll, L. Shulenburger, and M. D. Furnish, *Nat. Comm.* **12**, 876 (2021).

[61] J. Li, Q. Wu, J. Li, T. Xue, Y. Tan, X. Zhou, Y. Zhang, Z. Xiong, Z. Gao, and T. Sekine, Geophys. Res. Lett. **47**, e2020GL087758 (2020).

[62] D. C. Swift, T. Lockard, R. F. Smith, C. J. Wu, and L. X. Benedict, Phys. Rev. Research **2**, 023034 (2020).

[63] R. A. Fischer and A. J. Campbell, Am. Min. **95**, 1473 (2010).

[64] R. A. Fischer, A. J. Campbell, G. A. Shofner, O. T. Lord, P. Dera, and V. B. Prakapenka, Earth. Planet. Sci. Lett. **304**, 496 (2011).

[65] T. Komabayashi, J. Geophys. Res. Solid Earth **119**, 4164 (2014).

[66] M. Millot, S. Hamel, J. R. Rygg, P. M. Celliers, G. W. Collins, F. Coppari, D. E. Fratanduono, R. Jeanloz, D. C. Swift, and J. H. Eggert, Nat. Phys. **14**, 297 (2018).

[67] R. Redmer, T. R. Mattsson, N. Nettlemann, and M. French, Icarus **211**, 798 (2011).

[68] R. Boehler, Rev. of Geophys. **38**, 221 (2000).

[69] H. F. Wilson and B. Militzer, Phys. Rev. Lett. **108**, 111101 (2012).

[70] S. M. Wahl and B. Militzer, Earth Planet. Sci. Lett. **410**, 25 (2015).

[71] R. Musella, S. Mazavet, and F. Guyot, Phys. Rev. B **99**, 064110 (2019).

[72] S. Imada, K. Ohta, T. Yagi, K. Hirose, H. Yoshida, and H. Nagahara, Geophys. Res. Lett. **41**, 4542 (2014).

[73] S. Fu, Y. Yang, Y. Zhang, J. Liu, E. Greenberg, V. B. Prakapenka, T. Okuchi, and J.-Fu. Lin, Earth Planet. Sci. Lett. **503**, 1 (2018).

[74] F. Coppari, R. F. Smith, J. Wang, M. Millot, D. Kim, J. R. Rygg, S. Hamel, J. H. Eggert, and T. S. Duffy, Nat. Geosci. **14**, 121 (2021).